Conjugate Heat Transfer Predictions of a Combustor Heatshield Containing Pedestals

J.K. Luff and J.J. McGuirk
Dept. of Aero. and Auto. Engineering
Loughborough University
Loughborough LE11 3TU, UK

Abstract.

This paper reports an investigation into the use of CFD methods for modelling the combined fluid flow and heat transfer in a generic combustor heatshield geometry typical of current aeroengine designs. The study describes the development and testing of a conjugate heat transfer methodology, to allow the CFD code to predict the heat exchange in both fluid and solid regions of the solution domain simultaneously; special attention is given to continuity of heat flux at the fluid/solid interface. The heatshield cooling air is supplied via rows of jets that flow through holes in the backplate and impinge on the heatshield backside. An interesting phenomenon associated with these jets is investigated. It is noticed that under some conditions of heatshield flow, jet impingement leads to the model predicting a minimum in heat transfer coefficient, rather than a maximum, at the impingement point. It is shown, by predicting the measured Nusselt number distribution in a single impinging jet experiment, that this is a correct simulation, associated with the combined effects of low impingement height and low turbulence levels in the jet cores. The presence of pedestals on the impingement surface removes this effect by creating extra turbulence and enhancing conductive paths for heat transfer. A model for including the pedestals in both flow and heat exchange processes as a sub-grid-scale model in the CFD simulation is described. An illustrative calculation of the performance of the overall model for a realistic heatshield geometry is provided, indicating the predicted spatial variation of temperature on heatshield surfaces.

1. Introduction.

The estimation of the temperature field throughout the solid material of a gas-turbine combustor is an important element of the overall design process. Combustor wall temperatures are an essential factor which exert a strong influence on the induced thermal stress, material properties, and fatigue/creep calculations that limit the life of the combustor. The choice, and detailed design parameters, of the cooling air strategy are driven to a large extent by desired maximum metal surface temperatures, to be achieved using the minimum amount of cooling air. These considerations control, for example, the number and location of small film cooling slots, size of effusion patches containing thousands of small holes, use of cooling tiles with multiple pedestal arrays etc.

Accurate and early knowledge of the temperature field is particularly important in the case of combustor components which are highly stressed regions, or are subject to high heat transfer rates, such as the combustor heatshield. The heatshield sits in the head of the combustor, surrounding the fuel injector, and acts as a thermal shield against the extremely hot, radiating gases in the combustor primary zone. It must be cooled by air drawn through the cowl of the combustor, and minimising this cooling air, subject to allowable metal temperatures and heatshield stress fields, is a difficult design task. This task is further complicated by the complex geometry of this part of the combustor, see Fig. 1. The cooling airflows into, through (i.e. within the backplate and heatshield ‘sandwich’), and out of the heatshield front face, follow complex 3D flow paths. To maximise heat transfer rates, many heatshield designs make use of heat transfer augmentation devices such as large numbers of pin-fin pedestal arrays introduced between the heatshield and its backplate. It is therefore perhaps not surprising that the current design of this component is, to a large extent, empirically driven. The development of an accurate numerical model for prediction of the heat transfer processes within typical heatshield designs would be an extremely valuable tool, and this is therefore the focus of the work described in the present paper.

Paper presented at the RTO AVT Symposium on “Advanced Flow Management: Part B – Heat Transfer and Cooling in Propulsion and Power Systems”, held in Loen, Norway, 7-11 May 2001, and published in RTO-MP-069(I).

Report Documentation Page

Form Approved
OMB No. 0704-0188

1. REPORT DATE	2. REPORT TYPE	3. DATES COVERED
00 MAR 2003	**N/A**	**-**

4. TITLE AND SUBTITLE	5a. CONTRACT NUMBER
Conjugate Heat Transfer Predictions of a Combustor Heatshield Containing Pedestals	5b. GRANT NUMBER
	5c. PROGRAM ELEMENT NUMBER
6. AUTHOR(S)	5d. PROJECT NUMBER
	5e. TASK NUMBER
	5f. WORK UNIT NUMBER
7. PERFORMING ORGANIZATION NAME(S) AND ADDRESS(ES) **NATO Research and Technology Organisation BP 25, 7 Rue Ancelle, F-92201 Neuilly-Sue-Seine Cedex, France**	8. PERFORMING ORGANIZATION REPORT NUMBER
9. SPONSORING/MONITORING AGENCY NAME(S) AND ADDRESS(ES)	10. SPONSOR/MONITOR'S ACRONYM(S)
	11. SPONSOR/MONITOR'S REPORT NUMBER(S)

12. DISTRIBUTION/AVAILABILITY STATEMENT
Approved for public release, distribution unlimited

13. SUPPLEMENTARY NOTES
Also see ADM001490, presented at RTO Applied Vehicle Technology Panel (AVT)Symposium held in Leon, Norway on 7-11 May 2001, The original document contains color images.

14. ABSTRACT

15. SUBJECT TERMS

16. SECURITY CLASSIFICATION OF:			17. LIMITATION OF ABSTRACT	18. NUMBER OF PAGES	19a. NAME OF RESPONSIBLE PERSON
a. REPORT	b. ABSTRACT	c. THIS PAGE			
unclassified	**unclassified**	**unclassified**	**UU**	**14**	

Standard Form 298 (Rev. 8-98)
Prescribed by ANSI Std Z39-18

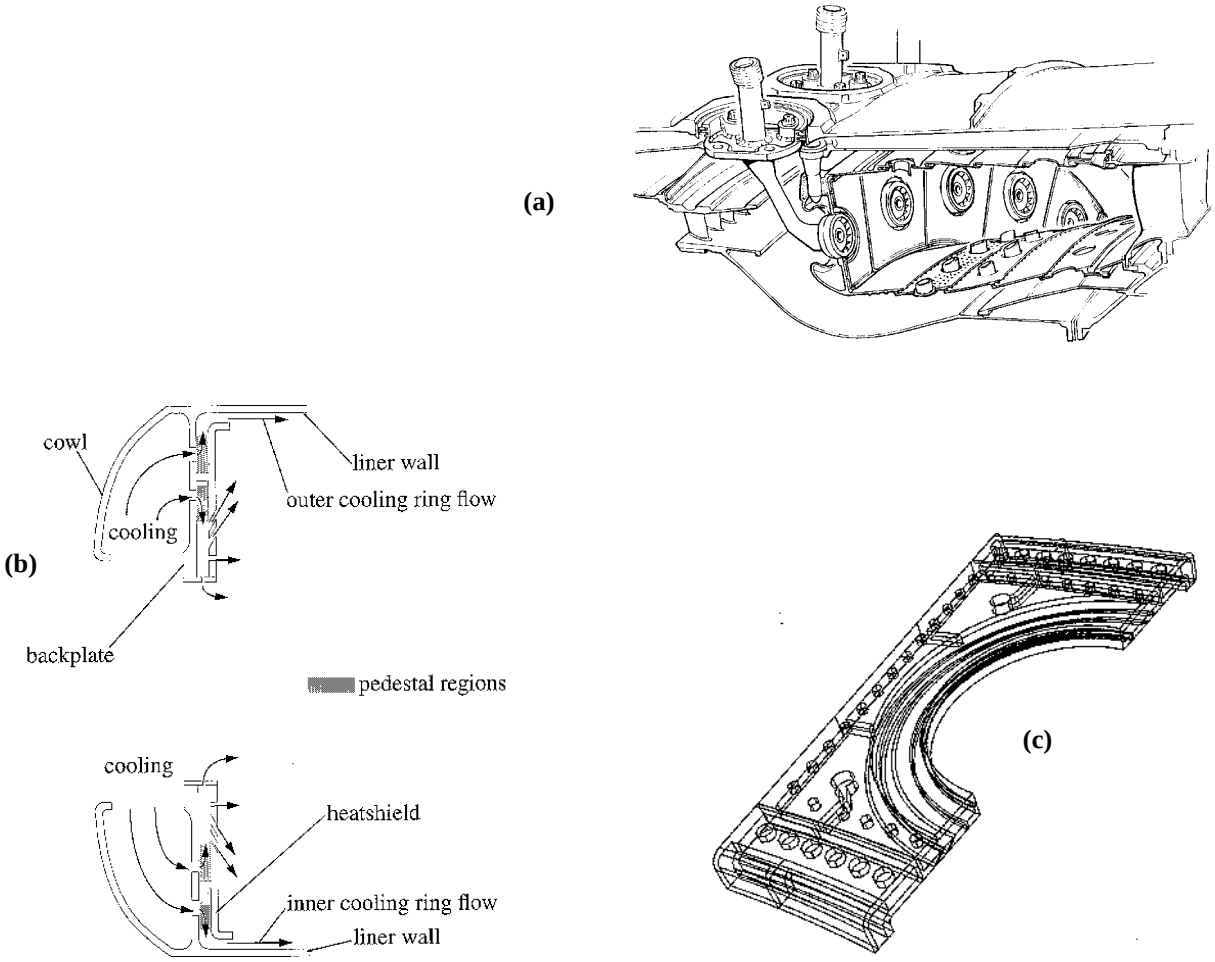

Figure 1. (a) combustor geometry, (b) heatshield cooling flow, (c) heatshield geometry.

It is extremely rare that combustor CFD calculations solve simultaneously for flow, reaction and conjugate heat transfer (i.e. convective/radiative heat input from the hot gases, convective cooling and conductive heat transfer through solid components). The usual approach (e.g. Krebs et al [1]) is to use measured, or estimated, wall temperatures as boundary conditions for the CFD predictions. Baldi et al [2] have provided perhaps the most complete description of a combined thermo-fluids and mechanical/materials stress analysis approach to life prediction of combustor liners, using a hybrid CFD/FEM model. The combustor geometry considered was, however, unrepresentative in its simplicity, and more emphasis was placed on the mechanical modelling of liner creep than on the accuracy of the heat transfer.

Crocker et al [3] present CFD calculations of a complete combustor geometry from compressor exit to turbine inlet (including flow predictions both external and internal to the combustor liner). These authors did include both convective and conduction heat transfer and hence produced liner wall temperature predictions. The combustor components did not, however, include any of the small-scale features mentioned above as this would have lead to prohibitively large meshes if these features were to be resolved by the grid. Full coupling of numerical fluid flow and conjugate heat transfer models is more common in the field of turbine blade cooling, e.g. Bohn et al [4]. Here similar challenges occur as described above in the combustor context, i.e. complex geometry, small scale heat exchange features (pedestals are often used in the thin trailing edge regions of blades), and minimising of cooling flows. Even in this application, however, internal pin-fin arrays are often excluded on grid resolution grounds, even though these contribute significantly to the heat transfer. Recently, Luff and McGuirk [5] have shown how a sub-grid-scale modelling approach may be adopted to take account of the pedestal heat transfer without unnecessarily enlarging the computational task.

The present paper continues reporting of the work begun in Ref. [5]. The same numerical techniques are used for heatshield and pedestal modelling. The opportunity is taken here to demonstrate the effectiveness of the approach adopted for conjugate heat transfer. In Ref. [5] a curious observation was made when the model was applied to a full heatshield calculation. This concerned the appearance of local minima in heat transfer coefficients at cooling air jet impingement points, most noticeable in the absence of pedestals. The prediction of this phenomenon is investigated and validated here before the model is again applied to the heatshield geometry with a small improvement made in the treatment of the effusion-type cooling holes which form a cooling film over the heatshield front surface.

The following section provides details of the mathematical model and numerical scheme used. This is followed by an investigation of jet impingement heat transfer for the short impingement height conditions relevant to heatshield flows. The 3D coupled fluid flow/conjugate heat transfer model is than applied to a combustor heatshield geometry generically similar to that found in current Rolls-Royce engine designs. Since the emphasis in the present paper is on description of the computational methodology, only 'isolated' heatshield calculations are presented, with simple but representative boundary conditions selected to represent combustor primary zone heat input.

2. Mathematical Model and Numerical Techniques.

2.1 Equations governing fluid flow.

The continuity and momentum equations are written in Cartesian tensor form. Steady mean flow is assumed. The approximation is also made that there is no internal heat generation and the temperature changes are sufficiently small that the fluid properties (in particular the density) may be assumed constant. (NB it is very easy to relax this assumption and allow the fluid density to be calculated from an ideal gas relation, but the simplification is made here as illustrative calculations only are presented). Under these conditions, the temperature becomes a passive scalar, but it is important to emphasise that the energy equation is eventually to be solved in both fluid and solid regions of the chosen solution domain.

$$\frac{\partial U_i}{\partial x_i} = 0 \tag{1}$$

$$\frac{\partial}{\partial x_j}\left(U_i U_j\right) = \frac{-1}{\rho}\frac{\partial P}{\partial x_i} + \frac{\partial}{\partial x_j}\left(\nu_{mol}\frac{\partial U_i}{\partial x_j} - \overline{u_i u_j}\right) \tag{2}$$

$$\frac{\partial}{\partial x_j}\left(U_j T\right) = \frac{\partial}{\partial x_j}\left(\frac{\lambda_{mol}}{\rho c_p}\frac{\partial T}{\partial x_j} - \overline{u_j t}\right) \tag{3}$$

Upper case letters indicate time-averaged mean values and lower case letters fluctuations about the mean. U_i is the velocity, P the pressure and T the temperature; ρ is the fluid density, c_p is specific heat and ν_{mol} and λ_{mol} represent the diffusive properties for momentum (kinematic viscosity) and heat transfer (conductivity) respectively. The standard high Reynolds number two-equation k-ε model and associated wall functions (Launder and Spalding [6]) are used; the Reynolds stresses and turbulent heat fluxes in Eqns. (2) and (3) are thus modelled via:

$$-\overline{u_i u_j} = \nu_t\left(\frac{\partial U_i}{\partial x_j} + \frac{\partial U_j}{\partial x_i}\right) - \frac{2}{3}k\delta_{ij} \tag{4}$$

$$-\overline{u_j t} = \frac{\lambda_t}{\rho c_p}\frac{\partial T}{\partial x_j} \tag{5}$$

$$\nu_t = C_\mu \frac{k^2}{\varepsilon} \tag{6}$$

Ref. [6] provides details on the full transport equations for k and ε.

If the energy equation is considered as a typical example, insertion of the turbulence closure scheme leads to:

$$\frac{\partial}{\partial x_j}\left(U_j T\right)=\frac{\partial}{\partial x_j}\left(\frac{\lambda_{eff}}{\rho c_P}\frac{\partial T}{\partial x_j}\right) \tag{7}$$

$$\lambda_{eff}=\lambda_{mol}+\lambda_t \qquad \left(\lambda_{mol}=\frac{\nu_{mol}}{\sigma_T},\lambda_t=\frac{\nu_t}{\sigma_{t,T}}\right) \tag{8}$$

Where the molecular and turbulent Prandtl numbers (σ_T and $\sigma_{t,T}$) are taken as 0.7 and 0.9 respectively.

In order to treat complex-shaped domains, the Cartesian versions of all transport equations are transformed into a general, curvilinear, non-orthogonal (ξ, η, ζ) co-ordinate system, defined by a grid generation process to fit the boundary shape of the desired geometry. The energy equation (7), for example, then assumes the form:

$$\begin{aligned}\frac{\partial}{\partial\xi}(UT)+\frac{\partial}{\partial\eta}(UT)+\frac{\partial}{\partial\zeta}(UT)=&\frac{\partial}{\partial\xi}\left[\frac{1}{|J|}\frac{\lambda_{eff}}{\rho c_P}\left(q_{11}\frac{\partial T}{\partial\xi}+q_{21}\frac{\partial T}{\partial\eta}+q_{31}\frac{\partial T}{\partial\zeta}\right)\right]\\&+\frac{\partial}{\partial\eta}\left[\frac{1}{|J|}\frac{\lambda_{eff}}{\rho c_P}\left(q_{12}\frac{\partial T}{\partial\xi}+q_{22}\frac{\partial T}{\partial\eta}+q_{32}\frac{\partial T}{\partial\zeta}\right)\right]\\&+\frac{\partial}{\partial\zeta}\left[\frac{1}{|J|}\frac{\lambda_{eff}}{\rho c_P}\left(q_{13}\frac{\partial T}{\partial\xi}+q_{23}\frac{\partial T}{\partial\eta}+q_{33}\frac{\partial T}{\partial\zeta}\right)\right]\end{aligned} \tag{9}$$

Where U, V and W now represent the mass-flux carrying velocity components and q_{ij} are the metric components of the Jacobian tensor J describing the transformation (for details see Ref. [7]).

The transformed equations are solved using a multi-block, structured grid, finite-volume formulation using an implicit pressure-correction method (for details see McGuirk and Spencer [11]). Boundary-fitted non-orthogonal grids were constructed using a grid-generator written to allow a CAD solid model interface (Eccles [12]). The solid model of the generic heatshield geometry shown in Fig. 1(c) was used to create a mesh in both fluid and solid regions of the heatshield; examples of the mesh, which consisted of 3 blocks and around 700,000 cells are given in Ref. [5].

2.2 Conjugate heat transfer.

The energy equation (9) is to be solved in both solid and fluid regions to allow conjugate heat transfer. In the solid region the velocity components are zero, so only the right hand side of Eqn. (9) remains, λ_t is clearly zero and λ_{mol} is now the solid material conductivity λ_s. It has been emphasised by other authors (e.g. Refs. [4] and [8]) that there are distinct advantages to being able to use identical numerical treatments for solving the energy equation in linked fluid/solid regions, but that this then requires careful attention to be paid to the heat flux evaluation at the fluid/solid interface. The fact that the diffusion coefficient changes sharply across a fluid/solid interface (sometimes by orders of magnitude) means that discontinuous temperature gradients result. Conventional discretisation practices for cell-centred finite-volume schemes are no longer accurate (see Patankar [9], who recommends using harmonic rather than arithmetic averaging for cell face conductivity). On highly non-orthogonal grids, as typically result from the geometrical complexity of heatshields, the formulation of the cross-derivative terms in Eqn. (9) also needs careful treatment. A numerical scheme has been developed that successfully addresses these issues. This is described in detail in Luff [10], but an indication of the concepts used, and evidence of their effectiveness, is provided here.

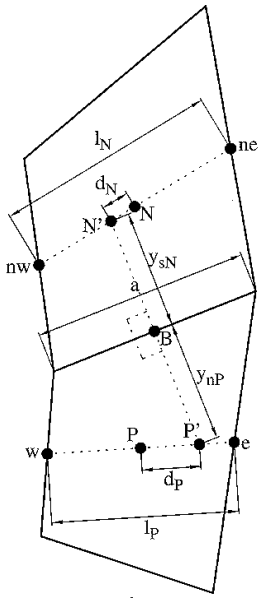

Figure 2. Heat transfer between two neighbouring finite-volume cells.

The methodology adopted is first described for two neighbouring solid regions with different thermal conductivities, and then extended to allow fluid/solid interfaces. This is done to enable the concept behind the method to be better understood, and because it facilitated the validation of the method on a test problem for which both an analytical solution and other authors' numerical results were available. The method is described using a 2D example, but has been generalised and applied to the fully 3D case.

Consider the diagram in Fig. 2; this illustrates a typical scenario for two neighbouring finite-volume cells (centred at P and N respectively) for a non-orthogonal grid. It is assumed that the material in cells P and N can have very different values of thermal conductivity (it is similarly assumed below that fluid/solid interfaces are arranged in the grid-generation step to coincide with cell boundaries). The heat flow rate across the north face of cell P may be written:

$$\dot{q}_{nP} = \lambda_P \frac{a}{y_{nP}} \left(T_B - T_{P'} \right) \tag{10}$$

where a and y_{nP} are geometric quantities calculated from grid information. The temperature at point P' may be calculated from (again d_P and l_P are grid calculated quantities):

$$T_{P'} = \frac{d_P}{l_P} \left(T_e - T_w \right) + T_P \tag{11}$$

This gives rise to the following expression for the heat flow rate at the north face of cell P, and a similar expression for the heat flow rate at the south face of cell N may be derived:

$$\dot{q}_{nP} = \lambda_P \frac{a}{y_{nP}} \left(T_B - T_P \right) - \lambda_P \frac{a d_P}{y_{nP} l_P} \left(T_e - T_w \right) \tag{12}$$

$$\dot{q}_{sN} = \lambda_N \frac{a}{y_{sN}} \left(T_B - T_N \right) + \lambda_N \frac{a d_N}{y_{sN} l_N} \left(T_{ne} - T_{nw} \right) \tag{13}$$

Since energy must be conserved at cell faces, even for discontinuous temperature gradients, $\dot{q}_{nP} = -\dot{q}_{sN}$ and an equation for the interface temperature T_B may be obtained:

$$T_B = \frac{\frac{\lambda_P}{y_P}T_P + \frac{\lambda_N}{y_N}T_N + \frac{\lambda_P d_P}{y_P l_P}(T_e - T_w) - \frac{\lambda_N d_N}{y_N l_N}(T_{ne} - T_{nw})}{\frac{\lambda_P}{y_P} + \frac{\lambda_N}{y_N}} \tag{14}$$

This is now used to eliminate T_B from the cell face heat flow rate expressions to give, for example:

$$\dot{q}_{nP} = \frac{\frac{\lambda_P}{y_{nP}}\frac{\lambda_N}{y_{sN}}}{\frac{\lambda_P}{y_{nP}} + \frac{\lambda_N}{y_{sN}}} a\left[(T_N - T_P) - \frac{d_N}{l_N}(T_{ne} - T_{nw}) - \frac{d_P}{l_P}(T_e - T_w)\right] \tag{15}$$

Note that this expression still contains unknown temperatures at cell faces (e.g. T_e, T_n, T_{ne} etc.). These are normally obtained by linear interpolation, but in regions where steep and discontinuous temperature gradients occur this can introduce significant errors. By examination of Eqn. (14) for the boundary temperature, it can be seen that this is a weighted average of the two cell temperatures either side of the boundary, plus some extra terms to account for differences in grid skewness on either side of the shared boundary. Neglecting these extra terms (since the cell face is fitted to the boundary shape, grid skewness is unlikely to change dramatically on either side of the boundary), a similarly weighted-average formulation can be used to provide relations for calculating the unknown face temperatures, for example:

$$T_e = \frac{\frac{\lambda_P}{y_{eP}}T_P + \frac{\lambda_E}{y_{wE}}T_E}{\frac{\lambda_P}{y_{eP}} + \frac{\lambda_E}{y_{wE}}} \quad , \quad T_{ne} = \frac{\frac{\lambda_N}{y_{eN}}T_N + \frac{\lambda_{NE}}{y_{wNE}}T_{NE}}{\frac{\lambda_N}{y_{eN}} + \frac{\lambda_{NE}}{y_{wNE}}} \quad \text{etc.} \tag{16}$$

The presence of the cell thermal conductivities in these relations means that a good approximation is obtained despite the discontinuous temperature gradients which can exist if the cell face corresponds to a material conductivity change or a solid/fluid interface. The same method may be used throughout the solution domain, since if conductivity is constant, it reduces to linear interpolation.

In order to validate this method, the test case for conjugate heat transfer recommended by Kelkar [8] has been calculated. This corresponds to heat conduction in a composite slab with internal heat generation; the problem possesses an analytical solution and also allows non-orthogonality errors to be assessed. Details of the geometry and the computational domain (with solution domain grid lines schematically indicated) are shown in Fig. 3.

An analytical solution for the non-dimensional temperature field $\theta(X,Y)$ for the case of a specified, spatially varying volumetric heat source is provided in Ref. [8] for a fixed conductivity ratio between the two regions shown, $C = \lambda_2/\lambda_1$. A numerical solution is found by solving the heat-conduction-only version of the energy equation over a computational domain formed by a parallelogram embedded symmetrically across the junction of the composite slab; the shape of the computational domain is selected to force a non-orthogonal grid with significant grid skewness. Solutions are obtained for a range of grids (5x10, 10x20, 20x40) with the boundary temperatures on the computational domain and the heat source at internal grid nodes fixed from the exact analytical solution. The normalised average error between the computed solution θ^c_{ij} at any grid node (i,j) and the exact solution θ_{ij} is calculated for each grid:

$$E = \frac{\Sigma\left|\theta^c_{ij} - \theta_{ij}\right|}{\Sigma\theta_{ij}} \tag{17}$$

Where the summation is taken over all internal grid nodes. Fig. 4 shows the variation of the normalised error for the 3 grids and for various values of conductivity ratio C.

Several comments can be made on these results. Firstly, for C = 1 the gradient of the decrease in error shows that the scheme is second-order accurate. As C increases, the errors grow and the formal second- order accuracy is lost due to the neglect of the extra terms in the interpolation. For very high C values, second-order accuracy returns since the importance of these extra terms diminishes. These observations are analogous to those made by Kelkar et al [8] in their prediction of this problem; it should be noted, however, that the present results for the error levels shown in Fig. 4 are about 50% of those given in Ref. [8] for the same grid density. This is due to the improved interpolation scheme for the cross-derivative terms suggested above in Eqn. (16).

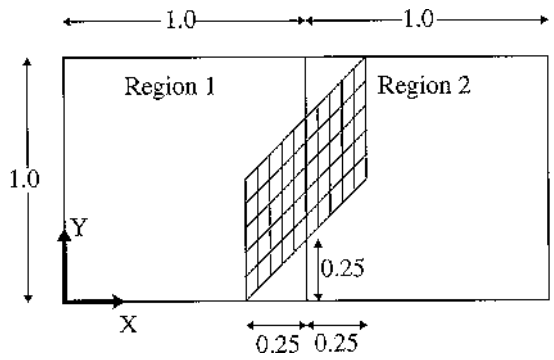

Figure 3. Geometry and solution domain for conjugate heat transfer test case.

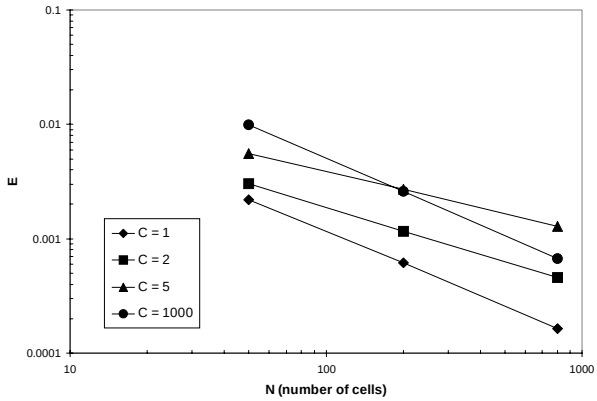

Figure 4. Normalised error in conjugate heat transfer test case for various grids and C values.

If convective fluid flow is present in one control volume and solid material conduction in the other (e.g. at the P/N cell interface in Fig.2), the method is easily adapted. For the high Reynolds number turbulence closure treatment adopted here, a log-law-based wall-function approach is used to specify one of the heat flows; for example, the heat flow at the north face of cell P is calculated via:

$$\dot{q}_{nP} = \frac{\rho c_P k_P^{0.5} C_\mu^{0.25}}{\sigma_{t,T}\left[\frac{1}{\kappa}\ln\left(\frac{E y_P k_P^{0.5} C_\mu^{0.25}}{\nu_{mol}}\right) + P_f\right]} a\left[\left(T_B - T_P\right) - \frac{d_P}{l_P}\left(T_e - T_w\right)\right] \tag{18}$$

Here k_P represents the turbulence energy at the near wall grid node, and C_μ, κ, E and P_f are constants taken from the standard high Reynolds number turbulence model (Ref. [6]). This is equivalent to the expression used in the conduction only case (Eqn. (12)), but with a modified or 'effective' value used for the 'cell' conductivity λ_P^{eff}, viz.:

$$\lambda_P^{eff} = \frac{y_{nP}\rho c_P k_P^{0.5} C_\mu^{0.25}}{\sigma_{t,T}\left[\frac{1}{\kappa}\ln\left(\frac{E y_P k_P^{0.5} C_\mu^{0.25}}{\nu_{mol}}\right) + P_f\right]} \tag{19}$$

the remainder of the analysis thus proceeds as before but using this effective value for λ_P.

2.3 Pedestal sub-grid-scale model.

To augment heat transfer between the hot front surface of the heatshield and the cooling air flowing in between the heatshield and backplate, use is commonly made of pin-fin type pedestals. The large number but small size of these would make it prohibitively difficult to resolve the flow around each pin and the heat transfer from each pin accurately in the finite-volume model. Luff and McGuirk [5] have shown how the main effects of the pedestals (in terms of extra pressure drop, extra turbulence generation and extra heat transfer) may be accounted for adequately using a sub-grid-scale model. This consists of adding extra terms into the momentum and turbulence equations and solving an extra energy equation to determine the local pedestal temperature (purely conduction, but with anisotropic

conductivity, allowing conduction only in the direction parallel to the pedestal axis). For example, the pedestal pressure drop, in regions of the mesh which are identified to the code as containing pedestals, is introduced on a cell- by-cell basis as an extra pressure gradient in the momentum equations:

$$R_{x_i} = \left(\frac{\partial P}{\partial x_i} \right)_{extra} = 0.5 \frac{1}{s_l} \rho f_{ped} V_{x_i,max} \left| V_{max} \right| \tag{20}$$

Here s_l is a geometric parameter of the pedestal geometry (streamwise pitch), V_{max} is the component of cell velocity normal to the pedestals (taking account of blockage), and f_{ped} is an empirical friction factor which describes the extra pressure loss per row of pedestals. This latter factor is taken from experimental work on flow over tube banks, where pressure loss data has been previously correlated by Zukauskas [13] in terms of the Reynolds number of flow over the pedestals, i.e.:

$$f_{ped} = \chi a \, Re_{ped}^{b} \tag{21}$$

χ, a, and b are empirical constants dependant on pedestal array geometry and layout. Similarly, an extra source term is included in the fluid energy equation (and an equivalent term of opposite sign in the pedestal energy equation) to account for pedestal-to-fluid heat transfer, and this is again empirically described using a Nusselt number correlation, also taken from Zukauskas[13]:

$$Nu_{ped} = 0.35 \left(\frac{s_t}{s_l} \right)^{0.2} Re_{ped}^{0.6} \, \sigma_T^{0.36} \tag{22}$$

This sub-grid-scale model was validated in Ref. [5] against experimental pressure loss and heat transfer data taken from Metzger et al [14]. The approach was shown to perform very well, in spite of the fact that the Zukauskas [13] empirical correlations were taken for long tubes rather than short pins, and from experiments that were far removed from the geometrical scenarios typical of heatshield pedestals.

3. Impinging jet heat transfer.

The cooling airflow in the heatshield application is metered through a series of round holes in the backplate, creating rows of jets impinging on the back surface of the heatshield (see Fig. 1). The diameter of these holes, and the backplate/heatshield separation, are such that these jets are at very small impingement heights, H/D. In earlier work on combustor heatshield heat transfer, Luff and McGuirk [5] noted the anomalous result that, in the absence of pedestals, local minima in heat transfer coefficients were predicted beneath these impinging jets, rather than the expected maxima. This aspect of heatshield heat transfer is further examined here.

Impinging jet heat transfer has been much studied in the past, and has been noted as a difficult problem for eddy viscosity turbulence models (see, for example, Craft et al [15]). These authors reported that, for the case of a single round impinging jet, the linear eddy viscosity k - ε turbulence model leads to spuriously high rates of turbulence energy generation near the impingement point, and consequently very high heat transfer rates, with Nusselt numbers around twice those measured experimentally (Ref. [16]). They recommended use of a Reynolds Stress Transport model to resolve this problem. Durbin et al [17] have also studied the same case and developed a three-equation turbulence model to achieve satisfactory predictions. The same author previously (Ref. [18]) developed a modification to the basic linear k - ε model (a time scale limiter) to remove the overproduction of k in stagnation flows. Luff and McGuirk [5] proposed that the low Nusselt numbers at impingement in their heatshield calculations were related to previously reported experimentally observed minima in impingement cooling flows at low values of H/D and with low turbulence levels in the jet core (see Ref. [19]). To test the validity of this proposal, for the particular turbulence model used here (and in Ref. [5]), the case of a single round impinging jet, as studied computationally in Refs. [15] and [17] and experimentally in Ref. [16], is predicted here.

Fig. 5 presents the predicted streamline pattern for the case selected for study, which represents the Re = 23,000, H/D = 2.0 case taken from the measurements reported in Ref. [16]. Following the practice of other authors (Refs. [15], [17]) the calculations are started upstream of the jet exit to allow some up-stream distortion of the jet conditions by the pressure field at impingement. Other boundary conditions are also as used by other authors', i.e. fully-developed velocity and turbulence profiles at entry to the jet pipe, and constant static pressure boundaries on the top and right hand sides of the solution domain (representing essentially entrainment and outflow boundaries as seen in Fig. 5).

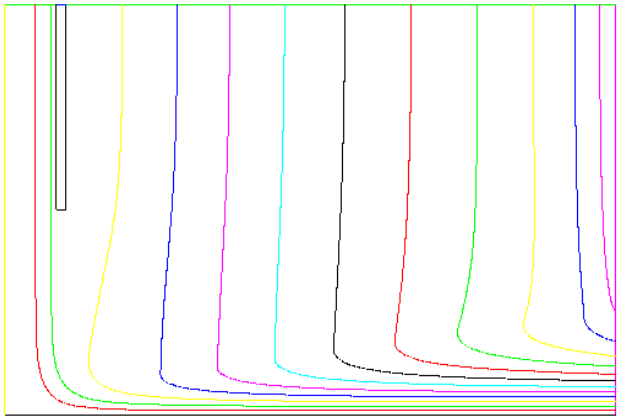

Figure 5. Streamline pattern, single impinging jet

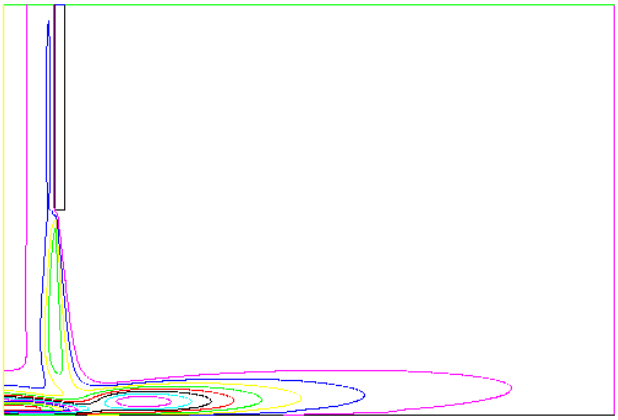

Figure 6. Turbulence energy contours, single impinging jet

The impingement process leads to the formation of a strong wall-jet flow, whose thickness grows away from impingement; the large k levels created by the high strain rates near stagnation are also very plain to see (Fig. 6), with the predicted maximum k value being 7.5% of the square of the mean jet velocity. Note the position of a secondary maximum in k just away from impingement. It is known that the heat transfer problem is computationally much more demanding than flowfield prediction, so a series of grid refinement tests have been carried out. Fig. 7 presents the predicted Nusselt number distribution along the impingement surface for two grids, where both axial and radial mesh refinement has been conducted. It is clear that the present solutions are certainly numerically accurate for heat transfer parameters.

It is very significant in Fig. 7 that not only are the present predictions numerically accurate, but they seem to represent better agreement with the experimental data than has previously been reported. Although the stagnation point Nusselt number is overpredicted, the 100% error obtained in Refs. [15] and [17] is not observed here. The reason for this is that the present results have been obtained with the high-Re wall function approach, rather than attempting to use a low-Re turbulence model and predict the flow all the way down to the wall as was the case in Refs. [15] and [17]. The y_+ value at the first cell next to the wall was kept greater than 30 for all the grids shown in Fig.7. It is clear that most of the overprediction of Nu seen in earlier work is a result of the low Re model reacting adversely to the enhanced k production near stagnation. When high-Re-model-based wall functions are used, although k is still overpredicted, this does not lead to a large error in Nu. The peak Nu value is actually slightly off-axis, and there is also the appearance of a further local increase in Nu in the region of the secondary maximum in k mentioned above. The use of the time-scale limiter recommended by Durbin [18] is shown in Fig. 8. This has the desired effect of reducing the peak levels of k at stagnation (maximum value now only 5.2% of jet velocity squared), and this brings down the peak Nu levels, to values actually slightly below those measured. The effect of the limiter is only active in the first jet diameter along the impingement wall.

With the basic model now validated as producing reasonable results for the experimental case considered in Ref. [16], a computational experiment was now performed, with the resulting Nusselt number distribution also included in Fig. 8. A change is made in the jet nozzle conditions; rather than

using fully-developed profiles, a flat velocity profile and uniform, low turbulence entry conditions were used (0.5% turbulence intensity and a length scale of D/10). It is very clear to see how, at this low impingement height, the impingement point Nusselt number now displays a local minimum (reduction by a factor of 3 to a level only 50% of the off-axis peak value), as observed in previous experiments (Ref. [19]) and full heatshield predictions at similar values of H/D (Ref. [5]).

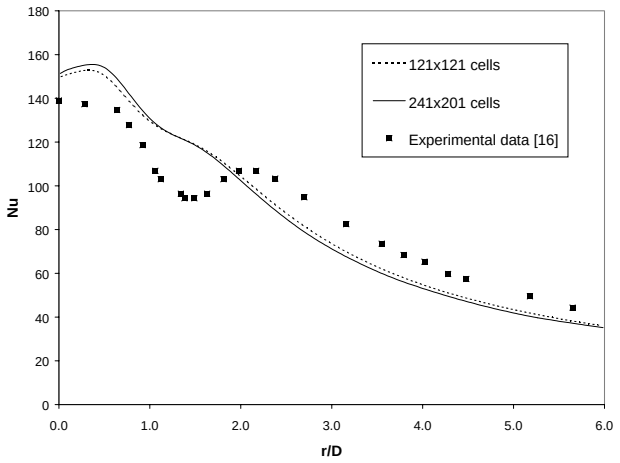

Figure 7. Nusselt number predictions (grid refinement).

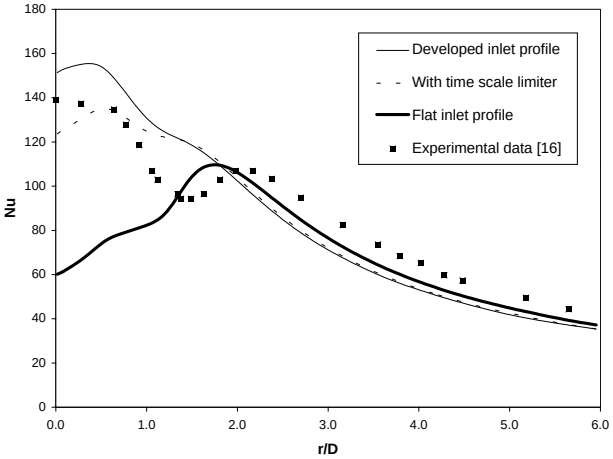

Figure 8. Nusselt number predictions (time scale limiter and jet condition effects).

4. Full heatshield heat transfer.

The complete model, as described in Section 2. above, has been applied to a generic heatshield heat transfer problem. The geometry used is described fully in Ref. [5] and is shown in Fig. 1; symmetry has been assumed about the heatshield centre plane. The cooling air enters through discrete feed holes in the backplate, with separate rows feeding the centre section and upper and lower sections. The air exits from the latter two sections, after flowing over pedestal arrays, as inner and outer cooling ring flows at the top and bottom of the main combustor. The airflow in the centre section exits mainly through the heatshield front face via 3 annular rings of small holes. In Ref. [5] these were represented for simplicity as 3 circular slots with the same geometric area as the multiple cooling holes. In the present calculations the opportunity has been taken to improve the modelling of this aspect. If the exit flows are treated as circular slots, it is believed that a reasonable representation is achieved of the flow conditions; it is obvious, however, that the use of circular slots provides a barrier to radial heat conduction paths, which are clearly present in the real multiple hole geometry. In the present calculations, a similar approach to that used to model pedestals at the sub-grid-scale level has been adopted to represent the individual metal regions between holes as ‘pin-fins’ in the slot regions, to allow radial heat conduction via the sub-grid-scale source terms containing the pin-fin temperature, calculated via an extra energy equation.

Numerical treatment and boundary conditions have otherwise reproduced those used in Ref.[5]; a uniform total pressure at all inlets, and fixed static pressure at all exits establishes the mass flow through the heatshield. Heat transfer boundary conditions correspond to a fixed temperature on the back surface of the backplate (and for all inlet airflows), at a level T_{in} typical of compressor exit flow. The thermal boundary condition on the front face of the heatshield was fixed as a uniform heat flux of 1 MW/m^2; it would be relatively easy to improve this condition by specifying a heat flux consistent with a convective and radiant heat input obtained from a separate combustor calculation, but it is believed that the simplified condition chosen is representative and sufficient to illustrate the methodology described here.

Fig 9 indicates the flow patterns obtained from the present model. The impinging and interacting jets in both the centre and inner/outer portions of the heatshield are a very distinctive feature, with the low

H/ D value now being very obvious. The effect of the presence of the pedestals on the flow pattern is mainly to smooth out the regions of recirculation between backplate and heatshield.
Figure 10 shows the predicted temperature field on the hotside of the heatshield. Fig. 10(left) represents predictions ignoring the radial conduction paths in the exit slot region and Fig. 10(right) shows the effect of modelling these in the manner described above.

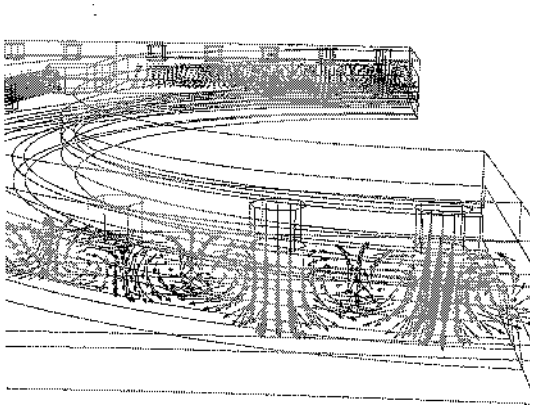

Figure 9. Velocity vectors in heatshield flow showing impingement

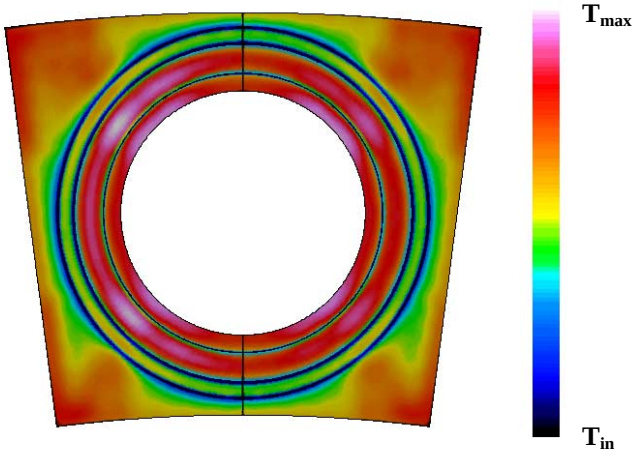

Figure 10. Heatshield hotside temperature contours (left) without radial conduction through slots and (right) allowing for radial conduction

It is noticeable that the high temperature regions correspond to regions with no pedestals or where local increases in metal thickness near mounting bosses and structural ribs create greater resistance to heat transfer. The allowance for radial conduction through the exit slot regions has not changed the overall temperature pattern, and it has reduced the peak temperatures by only around 1%.

5. Conclusions

The development and testing of a computational model for combustor heatshield heat transfer has been described. Due to the complex geometry of typical heatshields, it is inevitable that the 3D grids used to calculate the cooling flow through the component will contain regions of significant non-orthogonality. This makes the calculation of conjugate heat transfer through both fluid and solid regions difficult, unless special consideration is given to the solid/fluid interface treatment. A method hat can cope accurately with such grid distributions was described, and evidence provided of its suitability by calculating conduction through a composite material with highly skewed grids and large property variations. Heatshield flows contain multiple impinging jets of cooling air and this aspect of the problem was also investigated in some detail. For a single impinging jet, the use of the standard high Re-based k-ε turbulence model and log-law-based wall-functions was shown to provide better agreement with stagnation point Nusselt number distributions than was previously thought possible. The conditions appropriate to heatshield flows of low impingement heights and low jet core turbulence levels were shown to lead to minima in heat transfer coefficients at impingement. Finally, illustrations were provided of the application of the complete model, including a sub-grid-scale model for pedestals, to a realistic combustor heatshield geometry. Temperature distributions on the hotside were shown to provide detailed information about the location and level of hot spots. The model described is believed therefore to have significant value for the combustor heatshield design process and is a useful first step towards the more accurate modelling of combustor component stress fields and eventually combustor life prediction.

6. Acknowledgements.

This work was carried out as part of an EPSRC CASE research studentship. The project was part of work underway in the Rolls-Royce University Technology Centre in Combustion Aerodynamics at

Loughborough University. The authors would like to acknowledge useful discussions with colleagues at Loughborough, Rolls-Royce, and DERA.

7. References.

[1] Krebs, W., Walz, G., Hoffman, S., and Judith, H., "Detailed analysis of the thermal wall heat load in annular combustors", ASME paper 99-GT-134, 1999.
[2] Baldi, A., Vitale, E., Piccitto, U., "Combustor liner analysis by a thermo-mechanical integrated approach", ASME paper 99-GT-230, 1999.
[3] Crocker, D.S., Nickolaus, D., Smith, C.E., "CFD modelling of a gas-turbine combustor from compressor exit to turbine inlet", ASME Jnl. Of Eng. For Gas Turbines and Power, 122, pp 89-95, 1999.
[4] Bohn, D., Lang, G., Schonenborn, H., Bonhoff, B., "Determination of thermal stress and strain based on a combined aerodynamic and thermal analysis for a turbine nozzle guide vane", ASME paper 95-CTP-89, 1995.
[5] Luff, J.K. and McGuirk, J.J., "Numerical prediction of combustor heatshield flow and heat transfer with sub-grid-scale modelling of pedestals", ASME paper 2001-GT-0144, 2001.
[6] Launder, B.E. and Spalding, D.B., "The numerical computation of turbulent flows", Comp. Methods in Applied Mechs. And Engineering, 3, pp 269-289, 1974.
[7] Ferzinger, J.H. and Peric, M., "Computational methods for fluid dynamics", Springer Verlag, Berlin, Heidelberg, 1996
[8] Kelkar, K.M., Choudhury, D., Ambrosi, M., "Numerical method for the computation of conjugate heat transfer in non-orthogonal boundary-fitted co-ordinates", Numerical Heat Transfer, Part B, 20, pp 25-40, 1991.
[9] Patankar, S.V., "Numerical heat transfer and fluid flow", Hemisphere Publishing, 1980.
[10] Luff, J.K., " Numerical prediction of flow, heat transfer and stress fields in gas-turbine combustor components", Ph.D. thesis, Loughborough University, to be submitted, 2001.
[11] McGuirk, J.J. and Spencer, A., " CFD modelling of annulus/port flows", ASME paper 93-GT-185, 1993.
[12] Eccles, N.C., "Structured grid generation for gas-turbine combustors", Ph.D. thesis, Loughborough University, 2000.
[13] Zukauskas, A., "Heat transfer from tubes in crossflow", Advances in Heat Transfer, 8, pp 93-106, 1972.
[14] Metzger, D. E, Berry, R. A. and Bronson, J. P., "Developing Heat Transfer in Rectangular Ducts with Staggered Arrays of Short Pin Fins". ASME Jnl Heat and Mass Transfer, 104, pp 700-706, 1982.
[15] Craft, T. J. Graham, L. J. W. and Launder, B. E., "Impinging jet studies for turbulence model assessment - 2. An examination of the performance of four turbulence models". Int Jnl of Heat and Mass Transfer, 36, pp 2685-2697, 1993.
[16] Baughn, J.W.B. and Shimizu, S., "Heat transfer measurements from a surface with a uniform heat flux and an impinging jet". ASME Jnl of Heat Transfer, 111, pp 1096, 1989.
[17] Behnia, M., Parneix, S. and Durbin, P. A., "Prediction of heat transfer in an axisymmetric turbulent jet impinging on a flat plate". Int Jnl of Heat and Mass Transfer, 41, pp 1845-1855, 1998.
[18] Durbin, P. A., "On the k-epsilon stagnation point anomaly". Int Jnl of Heat and Fluid Flow, 17, pp 89-90, 1996.
[19] Gardon, R. and Akfirat, J.C., "The role of turbulence in determining the heat transfer characteristics of impinging jets", Int. Jnl. of Heat and Mass Transfer, 8, pp1261-1271, 1965.

Paper Number: 36

Name of Discusser: B. Simon, MTU Aero Engines Munich

Question:
How you determined heat transfer from the combustor hot side to the heat shield?

Answer:
Constant heat input of 1 MW/m^2 is prescribed on the hot side of the heatshield. This is a simplification but for methodology development it is sufficient. It will be possible in future to either more accurately prescribe heat input, or to extend the calculation domain into the combustor, so that convective heat transfer is predicted on the hot side whilst radiative heat input is prescribed.

This page has been deliberately left blank

Page intentionnellement blanche